



Symmetry-dependent phonon renormalization in monolayer MoS₂ transistor

Biswanath Chakraborty,¹ Achintya Bera,¹ D. V. S. Muthu,¹ Somnath Bhowmick,² U. V. Waghmare,² and A. K. Sood^{1,*}

¹*Department of Physics, Indian Institute of Science, Bangalore-560012, India*

²*Theoretical Sciences Unit, Jawaharlal Nehru Centre for Advanced Scientific Research, Bangalore-560064, India*

(Received 17 December 2011; published 6 April 2012)

A strong electron-phonon interaction which limits the electronic mobility of semiconductors can also have significant effects on phonon frequencies. The latter is the key to the use of Raman spectroscopy for nondestructive characterization of doping in graphene-based devices. Using *in situ* Raman scattering from a single-layer MoS₂ electrochemically top-gated field-effect transistor (FET), we show softening and broadening of the A_{1g} phonon with electron doping, whereas the other Raman-active E_{2g}^1 mode remains essentially inert. Confirming these results with first-principles density functional theory based calculations, we use group theoretical arguments to explain why the A_{1g} mode specifically exhibits a strong sensitivity to electron doping. Our work opens up the use of Raman spectroscopy in probing the level of doping in single-layer MoS₂-based FETs, which have a high on-off ratio and are of technological significance.

DOI: 10.1103/PhysRevB.85.161403

PACS number(s): 78.30.-j

The discovery of graphene¹ stimulated intense research activity due to the interesting fundamental phenomena it exhibits as well as the technological promise it holds in a broad range of applications ranging from sensors to nanoelectronics. The vanishing band gap of a single-layer graphene is a sort of a limitation in developing a graphene-based field-effect transistor with a high on-off ratio. This has spurred efforts to modify graphene to open up a gap and develop other two-dimensional (2D) materials such as MoS₂, WS₂, and boron nitride (BN), both experimentally and theoretically. Avenues to open up the gap through the modification of graphene include quantum confinement in nanoribbons,² surface functionalization,³ applying an electric field in the bilayer,^{4,5} deposition of graphene on other substrates such as BN,^{6,7} and B or N substitutional doping,⁸ which require fine control over the procedure of synthesis.

In contrast to graphene, single-layer MoS₂ consisting of a hexagonal planar lattice of Mo atoms sandwiched between two similar lattices of S atoms (S-Mo-S structure) with intralayer covalent bonding is a semiconductor with a direct band gap of ~ 1.8 eV, and is quite promising for field-effect transistor (FET) devices with a high on-off ratio. It has been shown that the luminescence quantum yield of monolayer MoS₂ is higher than its bulk counterpart.^{9,10} Recently a monolayer MoS₂ transistor¹¹ has been shown to exhibit an on-off ratio of $\sim 10^8$ and an electron mobility of ~ 200 cm²/V s. These values are comparable to silicon-based devices and make MoS₂-based devices worth exploring further. It is known that in a field-effect transistor, the carrier mobility is limited by scattering from phonons and the maximum current is controlled by hot phonons. Both these issues in a FET depend on electron-phonon coupling (EPC). Raman spectroscopy has been very effective to probe EPC for single-layer¹²⁻¹⁴ and bilayer graphene¹⁵⁻¹⁷ transistors by investigating the renormalization of the G and $2D$ modes as a function of carrier density.

Recent layer-dependent Raman studies of single and few layers of MoS₂ (Ref. 18) have shown that the frequency of the E_{2g}^1 phonon increases as the number of layers decreases, whereas the frequency of the A_{1g} phonon decreases.¹⁸ This

has been recently explained in terms of enhanced dielectric screening of the long-range Coulomb interaction between the effective charges with an increasing number of layers.¹⁹ For nondestructive characterization of carriers in a recently developed monolayer MoS₂ transistor,¹¹ Raman spectroscopy can be quite useful and requires precise knowledge and understanding of the phonon renormalization of a single MoS₂ layer as a function of carrier concentration. The temperature dependence of the mobility in n -type bulk MoS₂ had been attributed to the scattering of carriers by optical phonons that modulate thickness,²⁰ implying that the A_{1g} phonons with atomic displacements parallel to the c axis should be involved in controlling the mobility of the carriers.

In this Rapid Communication, we report an *in situ* carrier-dependent Raman study of a top-gated single-layer MoS₂ transistor, achieving a maximum electron doping of $\sim 2 \times 10^{13}$ /cm². The transfer characteristic of the top-gated device shows an on-off ratio $\sim 10^5$ and a field-effect mobility of 50 cm²/V s. We show that the A_{1g} mode shows a strong doping dependence; the phonon frequency decreases by 4 cm⁻¹ and the linewidth broadens by 6 cm⁻¹ for electron doping of 1.8×10^{13} /cm². The phonon frequency and linewidth of the E_{2g}^1 mode show much less dependence on carrier concentration. The difference in the behavior of these optical phonons are explained quantitatively using density functional theory (DFT).

Figure 1(a) shows a schematic of our experimental setup. Single-layer MoS₂ flakes were mechanically exfoliated from a bulk single crystal procured from M/s SPI Supplies and transferred on a 300-nm SiO₂ on a degenerately doped p -type silicon substrate (procured from M/s XT Wafer). After optical identification, the flake height is measured by contact-mode atomic force microscopy (AFM) to be 0.7 nm, in agreement with the S-Mo-S layer thickness [see Fig. 1(b)]. Standard electron-beam lithography and deposition were done to form ~ 50 -nm-thick Au contacts as the source (S), drain (D), and gate (G) electrodes. Room-temperature Raman spectra were recorded with 514.5-nm laser excitation with a Witec confocal spectrometer using a 50 \times long working distance objective. Laser power was kept below 1 mW to avoid sample heating.

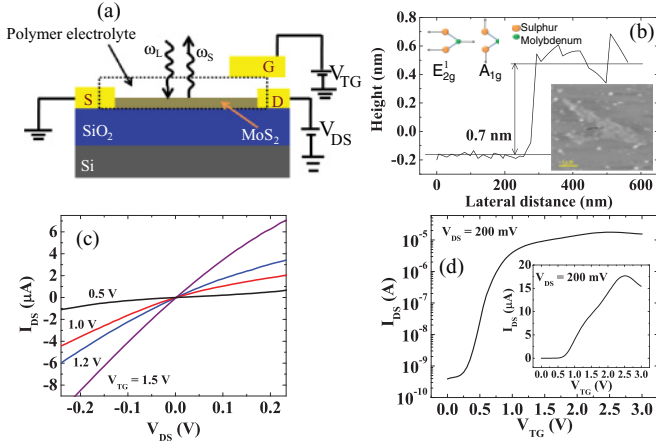


FIG. 1. (Color online) (a) Schematic of the experimental setup. Source, drain, and gate electrodes were marked as S , D , and G , respectively. The dotted box is the polymer electrolyte layer. (b) AFM height profile of the monolayer MoS_2 flake. Right inset: AFM image showing the dotted line along which the height profile is taken. The scale bar is $1 \mu\text{m}$. Left inset: Atomic displacements, indicated by arrows, corresponding to E_{2g}^1 and A_{1g} modes as viewed along the $[1000]$ direction. (c) I_{DS} - V_{DS} plot at various top-gate voltages V_{TG} . (d) I_{DS} as a function of V_{TG} at $V_{DS} = 200 \text{ mV}$. The on-off ratio was $\sim 10^5$ and the device mobility was estimated to be $50 \text{ cm}^2/\text{V s}$. The inset shows the transfer characteristic on a linear scale.

Electrical measurements were done with Keithley 2400 source meters. For top gating, we have used a solid polymer electrolyte comprising a mixture of LiClO_4 and polyethylene oxide (PEO) in a weight ratio 1:8. The solid polymer electrolyte as the gate material was chosen because of its high capacitance,⁵ enabling high carrier concentration with low gate voltage

($\leq 2 \text{ V}$). At the same time, because it is almost transparent, it allows us to perform *in situ* optical measurements with simultaneous electrical characterization. Figure 1(c) shows the drain-source current (I_{DS}) as a function of drain-source bias (V_{DS}) for a representative device of length (L) $2.5 \mu\text{m}$ and width (W) $1.5 \mu\text{m}$. A small nonlinearity may be due to the Schottky barrier at the contacts. The transfer characteristics of the device in Fig. 1(d) is plotted in a semilog scale. The on-off ratio for our device is $\sim 10^5$ and the low-field-effect mobility (μ) of our device was calculated ($\mu = \frac{L}{W} \frac{g_m}{V_{DS} C_{TG}}$) to be $50 \text{ cm}^2/\text{V s}$. Here g_m is the transconductance ($g_m = \frac{\partial I_{DS}}{\partial V_{TG}}$) of the device. Enhanced photoconductivity was observed when the incident laser beam was focused on the sample at gate voltages of 0.5, 1.0, 1.5, and 2.0 V, in agreement with recent reports.¹⁰ The photoconductive response was large at lower gate voltages but decreased at higher gate voltages when the conduction band started to become populated. Raman spectrum at each gate voltage was recorded only after the stabilization of the channel current. The threshold gate voltage V_T , at which the device switches from the “off” to the “on” state, was $\sim 0.1 \text{ V}$. The gate-induced electron concentration n is estimated using $ne = C_{TG}(V_{TG} - V_T)$. The value of C_{TG} is $1.5 \mu\text{F}/\text{cm}^2$. In brief, we extracted the value of top-gate capacitance C_{TG} from an experiment with a bilayer graphene transistor involving a dual-gate configuration.⁵ The back-gate dielectric was 300-nm SiO_2 . Several back-gate sweeps were done for fixed top-gate voltages. Since a maximum in the resistance corresponds to the charge neutrality point, the carrier concentration induced by both the gate voltages were equated to get the C_{TG} to be $1.5 \mu\text{F}/\text{cm}^2$. Since the electrolyte in the present experiments is same as in Ref. 5, we take this value in estimating n .

Figure 2(a) shows the evolution of zone-center phonon E_{2g}^1 and A_{1g} modes of the MoS_2 monolayer at different top-gate

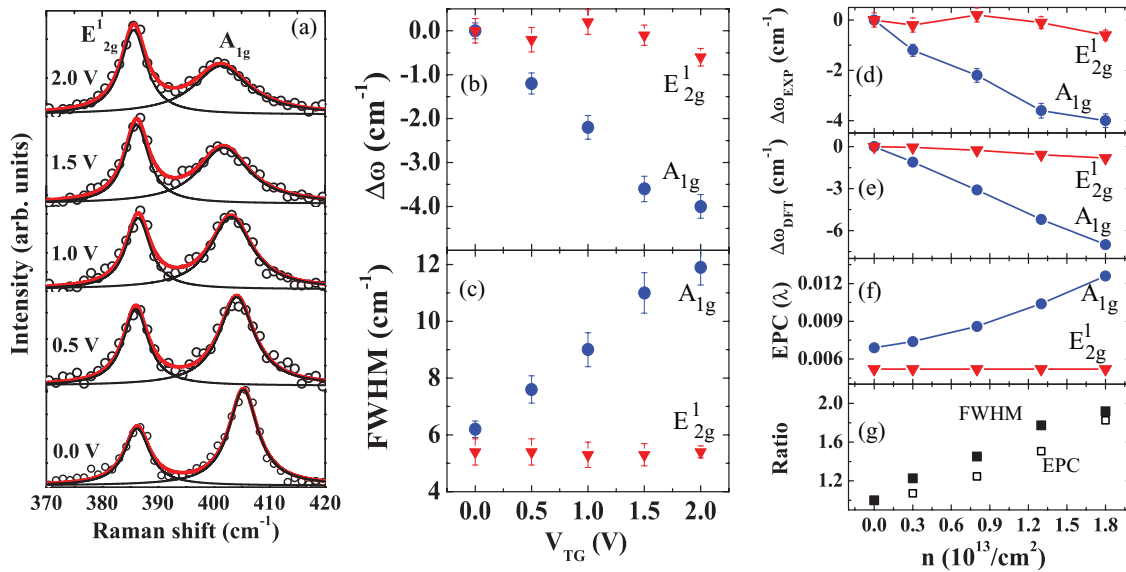


FIG. 2. (Color online) (a) Raman spectra of monolayer MoS_2 at different top-gate voltages V_{TG} . Open circles are experimental data points, the gray (red) lines are Lorentzian fits to the total spectrum, and the black lines are the Lorentzian fit to individual peak. Change in the (b) phonon frequency $\Delta\omega$ and (c) FWHM of A_{1g} and E_{2g}^1 modes as a function of V_{TG} . Change in zone center phonons $\Delta\omega$ of (d) from experiment and (e) from DFT calculations as a function of electron concentration n . (f) Electron-phonon coupling of A_{1g} and E_{2g}^1 modes as a function of n . (g) Ratio of EPC $[\lambda_{A_{1g}}(n \neq 0)/\lambda_{A_{1g}}(n = 0)]$ shown by open squares and phonon linewidth $[\text{FWHM}_{A_{1g}}(n \neq 0)/\text{FWHM}_{A_{1g}}(n = 0)]$ shown by solid squares as a function of n .

voltages. As depicted in the inset of Fig. 1(b), the A_{1g} phonon involves the sulfur atomic vibration in the opposite direction along the c axis (perpendicular to the basal plane), whereas for the E_{2g}^1 mode the displacement of Mo and sulfur atoms are in the basal plane. Line-shape parameters were obtained by fitting a sum of two Lorentzians to the data. Figures 2(b) and 2(c) show the shift of the mode frequencies and the corresponding full width at half maximum (FWHM), Γ , respectively, as a function of gate voltage. The dependence of the change in mode frequencies [$\Delta\omega = \omega(n \neq 0) - \omega(n = 0)$] on the carrier concentration (n) is shown in Fig. 2(d). For a maximum electron concentration of $1.8 \times 10^{13}/\text{cm}^2$, the A_{1g} mode frequency softens by 4 cm^{-1} , as compared to only $\sim 0.6 \text{ cm}^{-1}$ for the E_{2g}^1 mode. The linewidth of the A_{1g} mode increases significantly by $\sim 6 \text{ cm}^{-1}$ for the maximum doping achieved, whereas the linewidth of the E_{2g}^1 mode does not show any appreciable change. These results show that the A_{1g} phonon renormalization could be used as an *in situ* readout of the carrier concentration in MoS₂ devices. We will now quantitatively understand the different renormalization of the two modes A_{1g} and E_{2g}^1 due to the electron-phonon interaction.

Our calculations are based on first-principles density functional theory as implemented in the QUANTUM ESPRESSO package,²¹ a plane-wave basis set (70-Ry cutoff), and norm-conserving pseudopotentials (Rappe-Rabe-Kaxiras-Joannopoulos²²). The exchange-correlation energy of electrons is approximated with a local density approximation and a parametrized functional of Perdew and Zunger.²³ A monolayered form of MoS₂ is simulated using a periodic supercell, with a vacuum of $\sim 15 \text{ \AA}$ separating adjacent periodic images along the z direction. Integrations over the Brillouin zone were sampled with uniform $24 \times 24 \times 1$ and $48 \times 48 \times 1$ k -point meshes in the calculation of total energy and electron-phonon coupling, respectively.

Our calculations show that monolayer MoS₂ is a direct band-gap semiconductor with a band gap of 1.8 eV at the K point, in good agreement with known results.²⁴ Valence- and conduction-band edges primarily consist of Mo $4d$ states with some hybridization with S $3p$ states [see Figs. 3(a) and 3(b)]. In particular, states near the bottom of the conduction band near the K point have a character of the d_{z^2} state of Mo, and that at the top of the valence band has a d_{xy} character. We note that the charge density ($|\psi(r)|^2$) associated with each of these states has a full symmetry of the MoS₂ layer, which has

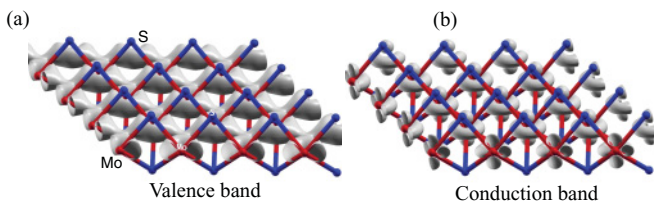


FIG. 3. (Color online) Contour plots (in light gray) of charge density ($|\psi(r)|^2$) (a) at the top of the valence, and (b) at the bottom of the conduction bands at the K point. While states near the top of the valence band consist of Mo $4d$ states with some hybridization with S $3p$ states, those near the conduction-band edge clearly have the character of the d_{z^2} state of Mo. The dark gray (red) and black (blue) spheres are Mo and sulfur atoms, respectively.

important consequences for electron-phonon coupling (to be elaborated on later).

We simulated electron doping in MoS₂ by adding a small fraction of electrons to its unit cell. Doping has contrasting effects on the frequencies of A_{1g} and E_{2g}^1 optic modes as shown in Fig. 2(e). While the former mode is found to soften significantly ($\sim 7 \text{ cm}^{-1}$ at $\sim 1.8 \times 10^{13}/\text{cm}^2$ doping), the latter is hardly affected, in very good agreement with our experimental results shown in Fig. 2(d). In order to understand this trend, we carry out a systematic study of electron-phonon coupling as a function of electron doping. The electron-phonon coupling (EPC) of a mode ν at momentum \mathbf{q} (with frequency $\omega_{q\nu}$) is calculated as²⁵

$$\lambda_{q\nu} = \frac{2}{\hbar\omega_{q\nu}N(\epsilon_f)} \sum_{\mathbf{k}} \sum_{mn} |g_{\mathbf{k}+\mathbf{q},\mathbf{k}}^{q\nu,ij}|^2 \times \delta(\epsilon_{\mathbf{k}+\mathbf{q},i} - \epsilon_f) \times \delta(\epsilon_{\mathbf{k},j} - \epsilon_f), \quad (1)$$

where ω and $N(\epsilon_f)$ is the phonon frequency and electronic density of states at the Fermi energy, respectively. The electron-phonon coupling matrix element is given by

$$g_{\mathbf{k}+\mathbf{q},\mathbf{k}}^{q\nu,ij} = \left(\frac{\hbar}{2M\omega_{q\nu}} \right)^{\frac{1}{2}} \langle \psi_{\mathbf{k}+\mathbf{q},i} | \Delta V_{q\nu} | \psi_{\mathbf{k},j} \rangle, \quad (2)$$

where $\psi_{\mathbf{k},j}$ is the electronic wave function with wave vector \mathbf{k} and energy eigenvalue $\epsilon_{\mathbf{k},j}$ for band j , and M is the ionic mass. $\Delta V_{q\nu}$ is the change in the self-consistent potential associated with a phonon of wave vector \mathbf{q} , branch ν , and frequency $\omega_{q\nu}$. Equation (2) defines the scattering of an electron from band j to band i due to the phonon ν with momentum \mathbf{q} . Our results in Fig. 2(f) show that the A_{1g} mode couples much more strongly with electrons than the E_{2g}^1 mode. This can be understood using a group theoretical analysis of symmetry. The A_{1g} mode has a symmetry of the lattice [the identity representation, i.e., the structural distortions in this mode do not break the symmetry of MoS₂—see the inset of Fig. 1(b)]. As a result, all electronic states can have a nonzero expectation value in Eq. (2) for the perturbation of the A_{1g} mode, giving a large electron-phonon coupling in Eq. (1). Electron doping leads to the occupation of the bottom of the conduction band at K -point states which have a character of d_{z^2} of Mo [see Fig. 3(b)]. The $|\psi(r)|^2$ of the states near the K point also transform according to the identity representation A_{1g} . Hence, changes in occupation of these states with electron doping yield a significant change in the EPC of the A_{1g} phonon. In contrast, the matrix element in Eq. (2) vanishes for the E_{2g}^1 mode (orthogonality of A_{1g} and E_{2g}^1 representations) and its coupling with electrons is weakly dependent on doping. Frey *et al.*²⁶ have put forward similar conclusions.

It is interesting to compare the EPC of MoS₂ with that of graphene. First of all, electron doping of about $1.8 \times 10^{13} \text{ cm}^{-2}$ results in the hardening of the G band of graphene¹⁴ by about 10 cm^{-1} and the softening of the A_{1g} mode of MoS₂ by about 4 cm^{-1} . The G -phonon renormalization occurs due to phonon-induced electron-hole (e - h) pair creations. For the G mode ($\mathbf{q} \sim 0$) in graphene, it involves e - h creation within a valley. Doping the graphene blocks the generation of phonon-induced e - h pairs and hence affects the phonon self-energy. Second, distortions of the structure with atomic

displacements of a G phonon lead to a mere shift of the center of the Dirac cone (and in the Fermi surface). If electrons follow these distortions, remaining in their ground state (adiabatic limit), their energy cost does not change with doping and hence doping would not result in any shift of frequency of the G band. However, it is the breakdown of the adiabatic approximation (the fact that electrons do not follow nuclear motion, remaining in their ground state) that is responsible for the energy cost and hardening of the G band with electron and hole doping.¹² Another way to explain this is in terms of the Kohn anomaly in graphene for a $\mathbf{q} = 0$ phonon which is weakened on doping. In contrast, in semiconducting MoS₂, phonon renormalization occurs within the adiabatic approximation. The electron doping results in the occupation of the antibonding states in the conduction band of MoS₂, making the bonds weaker, and the A_{1g} mode, which preserves the symmetry of the lattice, softens. While the EPC of the Raman mode at the Γ point of MoS₂ exhibits a strong dependence on doping, a similar dependence is seen for K -point phonons of graphene,²⁵ and our symmetry-based explanation applied here as well. We note that the latter transforms according to the identity representation of the symmetry group at (or near) the K point. The EPC argument applies to the linewidth as well. Two different mechanisms contribute to the phonon linewidth: (a) the EPC contribution (Γ^{EPC}) and (b) the contribution (Γ^{an}) arising from anharmonic effects.^{27,28} We can express $\Gamma = \Gamma^{\text{EPC}} + \Gamma^{\text{an}}$. The phonon linewidth Γ^{EPC} is proportional to EPC associated with

a particular mode.^{27,28} The increase in the A_{1g} linewidth is a result of the strengthening of electron-phonon coupling (λ) with doping [Figs. 2(c) and 2(f)]. Instead of the absolute values, we compare the ratios of Γ ($\Gamma_{n \neq 0} / \Gamma_{n=0}$) and EPC values ($\lambda_{n \neq 0} / \lambda_{n=0}$) for the A_{1g} mode [see Fig. 2(g)]. The Γ ratio follows the same trend as the EPC ratio, establishing that the increase in linewidth is due to increase in the electron-phonon coupling values (λ) with doping.

In summary, we have demonstrated that electron doping in single-layer MoS₂ results in softening specifically of its Raman-active A_{1g} phonon, accompanied by an increase in the linewidth of its Raman peak. In comparison, the other Raman mode with E_{2g}^1 symmetry is quite insensitive to electron doping. This is due to a stronger electron-phonon coupling of the A_{1g} mode than of the E_{2g}^1 mode, confirmed with first-principles DFT calculations and symmetry arguments. Our work shows how Raman scattering can be effectively used to characterize the level of doping in gated FET devices based on single-layer MoS₂ with a high on-off ratio of $\sim 10^5$ and having the potential to be used in digital electronics and sensors.

A.K.S. acknowledges funding from Department of Science and Technology, India, under the Nanomission grant. U.V.W. acknowledges funding from AOARD Grants No. FA2386-10-1-4062 and No. FA2386-10-1-4150 from the US Air Force. A.B. acknowledges support from the CSIR.

*Corresponding author: asood@physics.iisc.ernet.in

¹K. S. Novoselov, A. K. Geim, S. V. Morozov, D. Jiang, Y. Zhang, S. Dubonos, I. V. Grigorieva, and A. A. Firsov, *Science* **306**, 666 (2004).

²Z. Chen, Y. M. Lin, M. J. Rooks, and P. Avouris, *Physica E* **40**, 228 (2007).

³A. Cresti, A. L. Bezanilla, P. Ordejon, and S. Roche, *ACS Nano* **5**, 9271 (2011).

⁴J. B. Oostinga, H. B. Heersche, X. Liu, A. F. Morpurgo, and L. M. K. Vandersypen, *Nat. Mater.* **7**, 151 (2008).

⁵B. Chakraborty, A. Das, and A. K. Sood, *Nanotechnology* **20**, 365203 (2009).

⁶G. Giovannetti, P. A. Khomyakov, G. Brocks, P. J. Kelly, and J. van den Brink, *Phys. Rev. B* **76**, 073103 (2007).

⁷L. Ci, L. Song, C. Jin, D. Jariwala, D. Wu, Y. Li, A. Srivastava, Z. F. Wang, K. Storr, L. Balicas, F. Liu, and P. M. Ajayan, *Nat. Mater.* **9**, 430 (2010).

⁸L. S. Panchakarla, K. S. Subrahmanyam, S. K. Saha, A. Govindaraj, H. R. Krishnamurthy, U. V. Waghmare, and C. N. R. Rao, *Adv. Mater.* **21**, 4726 (2009).

⁹A. Splendiani, L. Sun, Y. Zhang, T. Li, J. Kim, C. Y. Chim, G. Galli, and F. Wang, *Nano Lett.* **10**, 1271 (2010).

¹⁰K. F. Mak, C. Lee, J. Hone, J. Shan, and T. F. Heinz, *Phys. Rev. Lett.* **105**, 136805 (2010).

¹¹B. Radisavljevic, A. Radenovic, J. Brivio, V. Giacometti, and A. Kis, *Nat. Nanotechnol.* **6**, 147 (2011).

¹²S. Pisana, M. Lazzeri, C. Casiraghi, K. S. Novoselov, A. K. Geim, A. C. Ferrari, and F. Mauri, *Nat. Mater.* **6**, 198 (2007).

¹³J. Yan, Y. Zhang, P. Kim, and A. Pinczuk, *Phys. Rev. Lett.* **98**, 166802 (2007).

¹⁴A. Das, S. Pisana, B. Chakraborty, S. Piscanec, S. R. Saha, U. V. Waghmare, R. Yiang, H. R. Krishnamurthy, A. K. Geim, A. C. Ferrari, and A. K. Sood, *Nat. Nanotechnol.* **3**, 210 (2008).

¹⁵J. Yan, E. A. Henriksen, P. Kim, and A. Pinczuk, *Phys. Rev. Lett.* **101**, 136804 (2008).

¹⁶A. Das, B. Chakraborty, S. Piscanec, S. Pisana, A. K. Sood, and A. C. Ferrari, *Phys. Rev. B* **79**, 155417 (2009).

¹⁷L. M. Malard, D. C. Elias, E. S. Alves, and M. A. Pimenta, *Phys. Rev. Lett.* **101**, 257401 (2008).

¹⁸C. Lee, H. Yan, L. E. Brus, T. F. Heinz, J. Hone, and S. Ryu, *ACS Nano* **4**, 2695 (2010).

¹⁹A. Molina-Sanchez and L. Wirtz, *Phys. Rev. B* **84**, 155413 (2011).

²⁰R. Fivaz and E. Mooser, *Phys. Rev.* **163**, 743 (1967).

²¹P. Giannozzi *et al.*, *J. Phys.: Condens. Matter* **21**, 395502 (2009).

²²A. M. Rappe, K. M. Rabe, E. Kaxiras, and J. D. Joannopoulos, *Phys. Rev. B* **41**, 1227 (1990).

²³J. P. Perdew and A. Zunger, *Phys. Rev. B* **23**, 5048 (1981).

²⁴H. S. S. R. Matte, A. Gomathi, A. K. Manna, D. J. Late, R. Datta, S. K. Pati, and C. N. R. Rao, *Angew. Chem. Int. Ed.* **49**, 4059 (2010).

²⁵C. Attaccalite, L. Wirtz, M. Lazzeri, F. Mauri, and A. Rubio, *Nano Lett.* **10**, 1172 (2010).

²⁶G. L. Frey, R. Tenne, M. J. Matthews, M. Dresselhaus, and G. Dresselhaus, *Phys. Rev. B* **63**, 2883 (1999).

²⁷M. Lazzeri, S. Piscanec, F. Mauri, A. C. Ferrari, and J. Robertson, *Phys. Rev. B* **73**, 155426 (2006).

²⁸N. Bonini, M. Lazzeri, N. Marzari, and F. Mauri, *Phys. Rev. Lett.* **99**, 176802 (2007).